JOURNAL OF APPLIED ELECTROCHEMISTRY 9 (1979) 517–525

Nucleation phenomena in the electrodeposition of lead onto glassy carbon electrodes

F. PALMISANO, E. DESIMONI, L. SABBATINI, G. TORSI

Istituto di Chimica Analitica, Università degli Studi, Via Amendola 173 Bari, Italy

Received 24 July 1978

The electrodeposition of lead onto a glassy carbon electrode from 0·1 M HCl solution has been studied mainly by potential step techniques. The early stages of metal deposition are shown to be controlled by a three-dimensional nucleation followed by hemispherical growth. The deposit morphology has been confirmed by scanning electron microscopy (SEM). Results obtained by linear sweep voltammetry are also reported and qualitatively interpreted according to the above-mentioned nucleation mechanism.

1. Introduction

Vitreous carbon has recently found extensive applications as an electrode material for analytical purposes. In particular it has been used, with or without a mercury film, for trace determination of heavy metals by anodic stripping voltammetry (ASV) and related techniques [1–3]. Recently Torsi [4] has employed this material as the crucible for *in situ* electrodeposition of heavy metals prior to their analysis by flameless atomic absorption spectrometry. In connection with all these applications the investigation of the electrodeposition mechanism of metals on vitreous carbon is of interest.

The electrodeposition phenomena were widely studied for various metals on different electrode materials both from aqueous solutions [5–11] and from molten salt systems [12–16].

In the present study a preliminary investigation on the electrodeposition of lead onto vitreous carbon from 0·1 M HCl solutions was performed mainly by potential step (single pulse) techniques. Results obtained by linear sweep voltammetry (LSV) were also collected and their abnormal features qualitatively explained in terms of the type of nucleation process involved in the electrodeposition reaction (see later).

The formation and growth of an electrodeposited phase is a complex process and several models have been proposed to describe the cathodic deposition of metals especially when the substrate and the metal are the same (for a review on this topic see [17]). In other cases it has been shown that electrodeposition reactions are associated with nucleation processes. In this respect the application of the classical vapour phase nucleation theory [18–20] to systems involving electrochemical deposition is relatively simple requiring a redefinition of the dimensionless 'supersaturation parameter', S in terms of the overpotential η, i.e.

$$S = \frac{zF}{RT}\eta \qquad (1)$$

The nucleation rate constant is now expressed by the following relationship

$$J = A \exp|-B/\eta^2| \qquad (2)$$

where B contains several constant terms [20]. According to this equation a critical overpotential (corresponding to a critical supersaturation for the homogeneous phase theory) is observed before the onset of the nucleation phenomena. The value of the critical overpotential is strongly dependent on the particular metal and substrate involved and usually ranges between 10–100 mV. Furthermore when a nucleation process takes place three different morphologies (one-dimensional, two-dimensional and three-dimensional as in the case of hemispherical growth) can be observed for the growth of nuclei formed on suitable nucleation sites. Whatever the growth morphology two different regimes can be established. For the first one

0021–891X/79/040517–09 $02·90/0

the rate-determining step is represented by the metal incorporation into the growth point; for the second one the rate-determining step is the mass transfer of the depositing metal ions towards the surface of the growth nucleus. In this latter case and the one relevant to the present study, Astley, Harrison and Thirsk [5] have derived the potentiostatic current–time transient for a diffusion controlled three-dimensional nucleation process. In terms of linear diffusion the current–time relationship for the growth of N_0 nuclei is given for instantaneous nucleation by

$$I(t) = \frac{8N_0zFM^2C^3D^{3/2}}{\rho^2\pi^{1/2}}t^{1/2} \qquad (3)$$

and for progressive nucleation by

$$I(t) = \frac{16K_nN_0zFM^2C^3D^{3/2}}{3\rho^2\pi^{1/2}}t^{3/2}. \qquad (4)$$

In these equations K_n is the rate constant (s^{-1}) for the formation of nuclei, M and ρ are the molecular weight and the density of the depositing metal, D and C are the diffusion coefficient and the concentration of the electrodepositing species, t is the time and all the other terms have their usual meaning in electrochemistry. Equations 3 and 4 have been modified by Hills *et al.* [13] in terms of spherical diffusion to the growth nucleous surface. Equations 3 and 4 are now respectively

$$I(t) = \frac{zFN_0\pi M^{1/2}(2D)^{3/2}C^{3/2}}{\rho^{1/2}}t^{1/2} \qquad (5)$$

$$I(t) = \frac{4zFK_nN_0\pi M^{1/2}D^{3/2}C^{3/2}}{3\rho^{1/2}}t^{3/2}. \qquad (6)$$

As it can be seen the equations obtained assuming planar or spherical diffusion differ from one another mainly in terms of the concentration dependence while the time dependence is the same. Thus the analysis of the current–time transient at controlled applied overpotential can give consistent indications on the presence of the above-mentioned nucleation process.

2. Experimental

For all the experiments a conventional three electrode system was used. The working electrode was prepared by fitting a vitreous carbon rod (3 mm in diameter) in a Teflon holder of 12 mm in diameter. The exposed electrode surface was polished to a mirror finish with alumina powder (particles dimension 1 μm). The counter electrode was a platinum foil of about 3 cm^2. All the potentials reported in this paper are referred to a saturated calomel reference electrode connected through a Luggin capillary. Overpotential values are calculated with respect to the potential of a lead wire dipped in the test solution although the equilibrium potential (relevant to the Pb/Pb^{2+} couple) calculated on the basis of the simple Nernst equation applied to the bulk concentration of Pb^{2+} ions was not experimentally verified. The discrepancy is to be ascribed to the existence, in a 0·1 M HCl solution, of the $PbCl^+$ complex together with the Pb^{2+} ions. As previously reported [21] the concentrations of Pb^{2+} and $PbCl^+$ are of the same order of magnitude and the diffusion coefficients of the two species are equal within about 5%. The Nernst equation becomes

$$E_{eq} = E^{0\prime} + RT/nF \ln f_{Pb^{2+}}C \qquad (7)$$

where $C = C_{Pb^{2+}} + C_{PbCl^+}$ and $E^{0\prime}$ is related to the standard potential E^0 for the simple ion by the relationship

$$E^{0\prime} = E^0 + RT/nF \ln K'/I + K' \qquad (8)$$

where $K' = Kf_{PbCl^+}/C_{Cl^-}f_{Pb^{2+}}f_{Cl^-}$, K is the dissociation constant of $PbCl^+$ and f the activity coefficient of the indicated species.

The voltammetric experiments were performed by an AMEL 'Electrochemolab' equipped with a Hewlett–Packard X–Y recorder. In some experiments a PAR 174 Polarographic Analyzer was used.

3. Results and discussion

3.1. *Linear sweep measurements*

Typical voltammograms (recorded at different potential scan rate) relevant to the electrodeposition of lead at a glassy carbon electrode are shown in Fig. 1 (curves a and b). In the same figure a′ and b′ represent the theoretical curves [22–24] calculated for a simple diffusion controlled process involving an insoluble product. The diffusion coefficient used in the calculations was obtained from potential step measurements

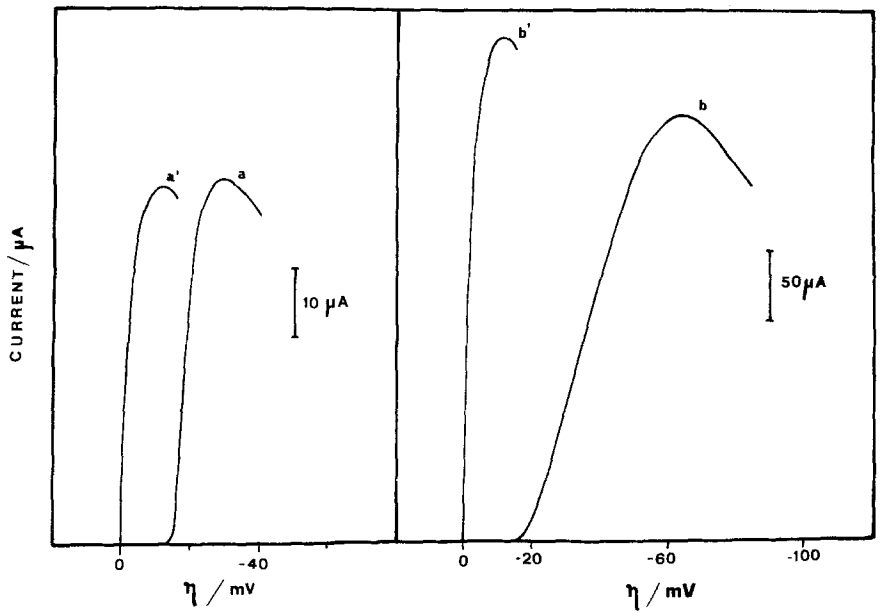

Fig. 1. Theoretical and experimental peak voltammograms for the reduction of Pb^{2+} in 0·1 M HCl solution at different scan rates v. $[Pb^{2+}] = 7{\cdot}20 \times 10^{-3}$ M; electrode area $7{\cdot}07 \times 10^{-2}$ cm^2. (a), (b) Experimental curves at 1 mV s^{-1} and 50 mV s^{-1} respectively. (a'), (b') Theoretical peak curves for a reversible deposition of an insoluble product.

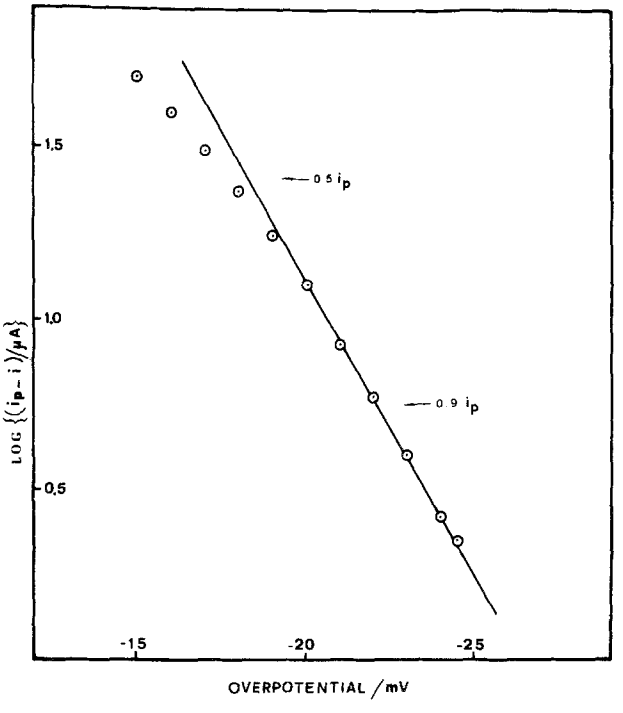

Fig. 2. Plots of log $(i_p - i)$ versus the applied overpotential η relevant to the peak voltammogram a of Fig. 1. The experimental points are compared with the theoretical slope (continuous line).

Table 1. Experimental values of the peak width ($E_p - E_{p/2}$) for the reduction of Pb^{2+} in 0·1 M HCl solution at vitreous carbon electrode

Scan rate (mV s^{-1})	($E_p - E_{p/2}$) (V)
1	0·011
5	0·014
20	0·019
50	0·027
	theoretical 0·010

(*vide infra*). An important feature is immediately evident i.e. the experimental reduction peak is shifted to negative potentials with respect to the theoretical one, the shift depending, for a given electrode material, on the scan rate and on the Pb^{2+} concentration.

A typical analysis log ($i_p - i$) versus E relevant to a reduction peak recorded at a slow scan rate (up to 5 mV s^{-1}) is shown in Fig. 2. It can be seen that the continuous line presenting [20] the slope $2{\cdot}2\,nF/RT$ (which characterizes a reversible process) overlaps the experimental points within the range 0·75–0·95 i_p and not within the range 0·5–0·9 i_p as required by the theory. Furthermore, on increasing the potential scan rate these plots become more and more bent and, as shown in Fig. 1 and Table 1, the peak width ($E_p - E_{p/2}$) becomes larger than the theoretical value [25] ($-0{\cdot}77\,RT/nF$).

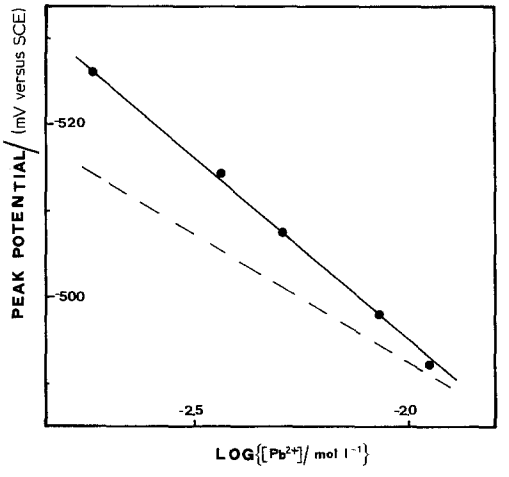

Fig. 3. Plot of the peak potential versus the logarithm of Pb^{2+} concentration for the reduction of lead in 0·1 M HCl. Peak voltammograms recorded at 50 mV s^{-1}. Dotted line represents the theoretical slope.

In Fig. 3 the peak potential is reported versus the logarithm of lead concentration. A linear dependence is observed but the slope is different from that predicted by theory [25] for a reversible metal deposition (dotted line) on the basis of the relationship

$$E_p = E^0 - 0{\cdot}218/n + 2{\cdot}3RT/nF \log C \quad (9)$$

where E^0 is the formal potential and the other symbols have their usual meaning in electrochemistry.

These results suggest that the electrodeposition of lead onto vitreous carbon proceeds irreversibly. This is confirmed by the dependence of peak potential and peak current on the scan rate v. A typical plot of E_p versus log v is reported in Fig. 4 for a given concentration of Pb^{2+}. The linear dependence of E_p on log v predicted [22] for an irreversible process is obeyed only at lower sweep rates. Since the ohmic overpotential is only a few mV even at the highest currents one can conclude that the deviation from linearity observed at sweep rates higher than 50 mV sec^{-1} must be ascribed to additional kinetic factors involved in the electrodeposition process (*vide infra*).

In Fig. 5 i_p is plotted versus $v^{1/2}$ for different Pb^{2+} concentrations. As it can be seen the plots are not strictly linear and do not pass through the origin as expected for a simple diffusion controlled process. The best straight lines in Fig. 5 were used to evaluate apparent diffusion coefficients for Pb^{2+} (see Table 2).

3.2. *Potential step measurements*

Typical current–time transients recorded at different overpotentials for a $[Pb^{2+}] = 8{\cdot}44 \times 10^{-3}$ M are shown in Fig. 6. At low cathodic overpotentials, in accordance with the linear sweep voltammetry, no reduction process can be observed but only a capacitive decay is apparent. At higher overpotentials corresponding to the foot of the peak voltammogram the reduction current increases, reaches a maximum and finally decays with time as expected for a simple diffusion process. For the sake of clarity this last part of the curves is not reported in the figure. At a given concentration the rising portions of the current–time transients are the shorter the higher the applied overpotential. At sufficiently cathodic overpotentials the rising

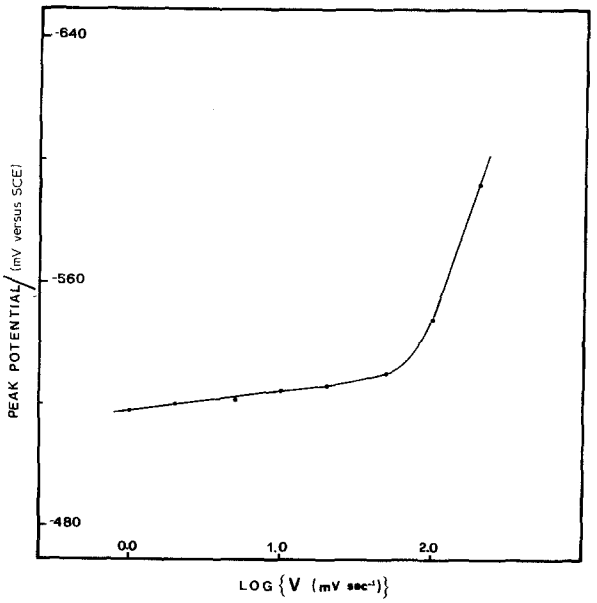

Fig. 4. E_p versus log v for the reduction of Pb^{2+} in 0·1 M HCl solution. $[Pb^{2+}] = 1{\cdot}81 \times 10^{-3}$ M.

portion is so short that it cannot be detected on a pen recorder and the usual diffusion controlled behaviour (i–$t^{-1/2}$ linear relationship) is observed. From such i–t curves recorded at an applied overpotential of − 200 mV the diffusion coefficient of Pb^{2+} was calculated and reported in Table 2.

3.3. *Mechanistic considerations*

The particular shape of the current–time transients strongly suggests that a nucleation process is involved in the electrodeposition of lead. Thus the first part of each transient is largely a charging current which decays during the process of nucleation. The rising portion reflects the increase in current because each independent nucleus grows in size and consequently increases the total area of the electro-active lead surface. In the later stages of the transients the diffusion zones around the nuclei overlap and one diffusion layer is formed, the shape of which will depend on the electrode geometry; consequently the current

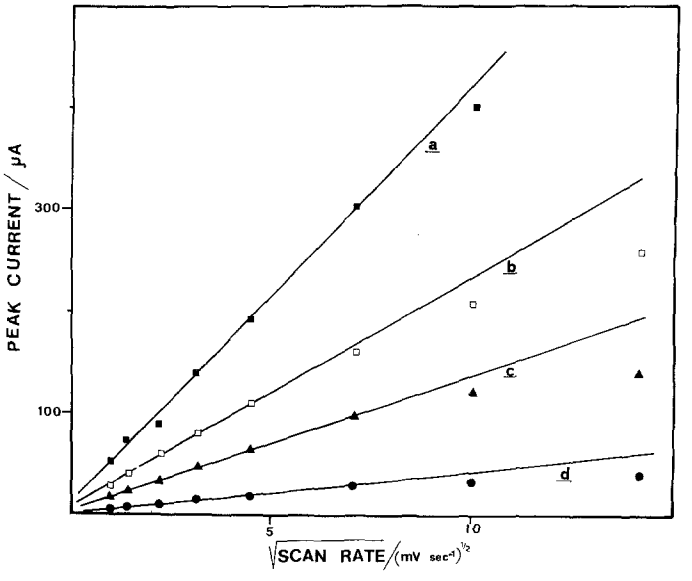

Fig. 5. Peak currents versus $v^{1/2}$ for the reduction of Pb^{2+} in 0·1 M HCl at different concentrations of lead:
(a) $[Pb^{2+}] = 7{\cdot}20 \times 10^{-3}$ M;
(b) $[Pb^{2+}] = 3{\cdot}62 \times 10^{-3}$ M;
(c) $[Pb^{2+}] = 1{\cdot}81 \times 10^{-3}$ M;
(d) $[Pb^{2+}] = 5{\cdot}00 \times 10^{-4}$ M.
Electrode area $7{\cdot}07 \times 10^{-2}$ cm^{-2}.

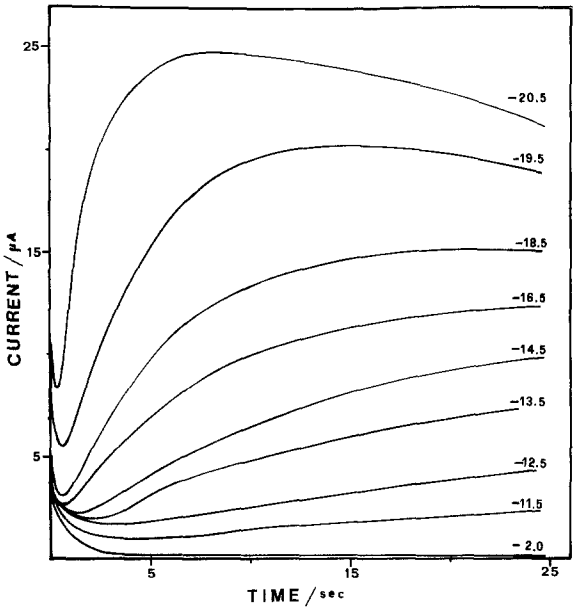

Fig. 6. Potentiostatic current–time transients for the deposition of lead onto vitreous carbon from $8{\cdot}44 \times 10^{-3}$ M $Pb(NO_3)_2$ in 0·1 M HCl at the indicated overpotentials (in mV). Electrode area $7{\cdot}07 \times 10^{-2}$ cm^2.

falls and approaches that corresponding to the diffusion controlled process. Furthermore the most pronounced minimum in the early region of the single pulse transients clearly shows that the nucleation kinetic is the rate-determining step in the electrodeposition process. An analysis of the rising portion of the transients shows that a linear i–$t^{1/2}$ relationship is observed (see Fig. 7). This result suggests, according to Equations 3 or 5, that the particular process involved is the one of an instantaneous three-dimensional nucleation with hemispherical growth. Direct evidence for this model was obtained by scanning electron microscope examination of the electrode surface (Figure 8). The spherical symmetry of the nuclei is evident as well as the fact that they have approximately the same dimensions as required for an instantaneous nucleation. An overlap between some neighbouring nuclei is also evident.

Table 2. A comparison between the diffusion coefficient values of Pb^{2+} obtained with different techniques

$[Pb^{2+}]$ (× 10^3 M)	*Diffusion coefficients* (× 10^5 cm^2 s^{-1})	
	Peak voltammetry	*Chronoamperometry*
0·50	1·37	–
1·81	0·96	–
3·37	–	0·96
3·62	0·74	–
5·06	–	1·01
7·20	0·61	–
8·44	–	0·92

The plots i–$t^{1/2}$ reported in Fig. 7 have different intercepts on the time axis and different slopes both depending on the overpotential. These experimental findings do not agree with the indication of Equations 3 and 5, i.e. zero intercept and no overpotential dependence. The intercept on the time axis can be explained [13] in terms of an 'induction period' (or time lag) necessary before the nucleation can proceed. As for the overpotential dependence of the slope of the i–$t^{1/2}$ plots this implies that the number of the nucleation sites is overpotential dependent and consequently there is a distribution of nucleation sites of different energies which nucleate at different overpotentials [8]. In this respect it can be interesting [26–28] to calculate the number of these sites in order to evaluate the nucleation rate constant. An attempt can be made to estimate the number of nuclei by a visual counting on micrographs [7, 29–33]. This is, however, an *ex situ* method which suffers from uncertainties depending on electrodes handling and on the fact that the nuclei must be appreciably large to be optically visible so that they can be the result from the condensation of smaller

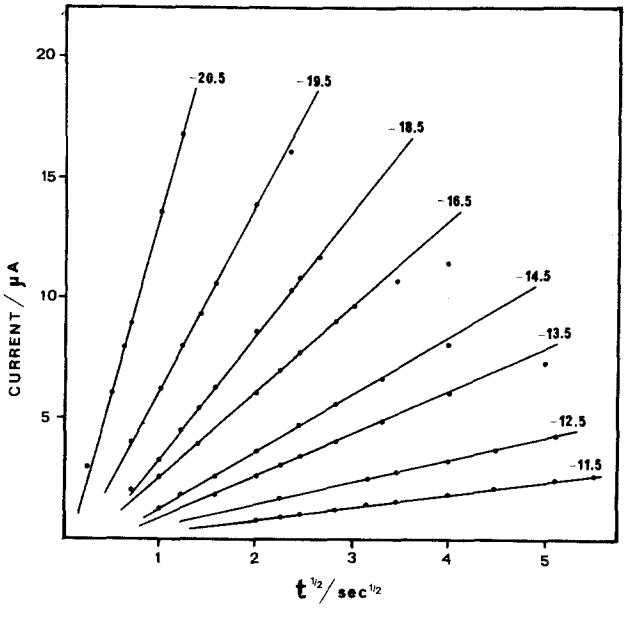

Fig. 7. Current versus $t^{1/2}$ plots for the growth of lead nuclei on vitreous carbon from 0·1 M HCl solution at the reported overpotentials (in mV). Data taken from Fig. 6.

ones. The number density of lead nuclei, N_0/cm^2, can be also evaluated by the slope of the i–$t^{1/2}$ plots or by a computer simulation method [34]. Table 3 gives the values obtained at different overpotentials by using both Equations 3 and 5. As it can be seen the use of different equations leads to large discrepancies in the calculated number densities. Furthermore any effort to verify experimentally the C^3 (Equation 3) or the $C^{3/2}$ (Equation 5) dependence systematically failed,

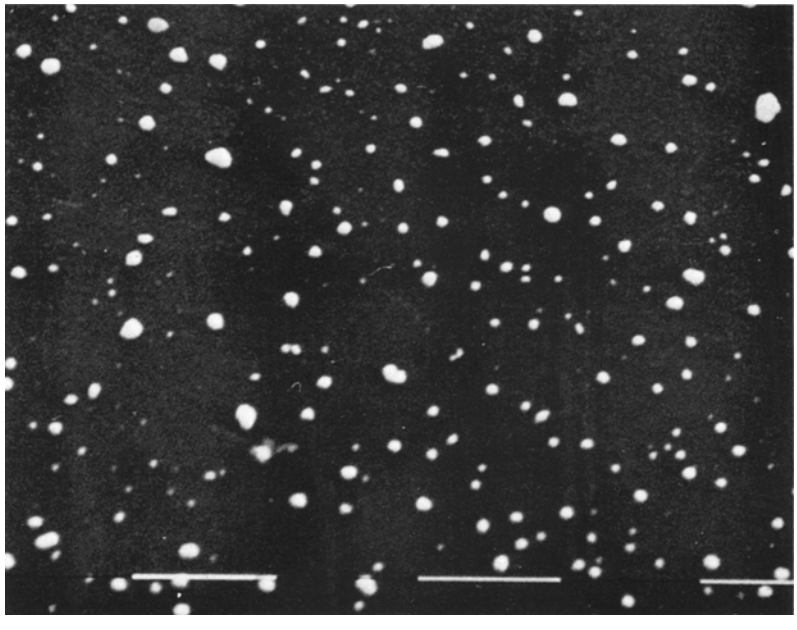

Fig. 8. Scanning electron micrograph of lead deposited on vitreous carbon at an applied overpotential of − 16 mV from 0·1 M HCl solution containing a $Pb(NO_3)_2$ concentration of $6{\cdot}72 \times 10^{-3}$ M. The deposit has been grown for 15 s, i.e. in the range of validity for Equation 3 or 5. The marker on the photograph is 1 μm.

Table 3. Number densities of lead nuclei, $N\,cm^{-2}$, evaluated by using Equations 3 and 5. Data taken from Fig. 7

		Number density	
Overpotential (mV)	$dI/dt^{1/2}$ ($\times 10^6$ $A\,s^{-2}$)	*Equation 5* ($N\,cm^{-2} \times 10^{-3}$)	*Equation 3* ($N\,cm^{-2} \times 10^{-9}$)
−11·5	0·58	1·54	1·58
−12·5	0·91	2·41	2·48
−13·5	1·57	4·16	4·28
−14·5	2·37	6·29	6·47
−16·5	3·58	9·49	9·76
−18·5	4·55	12·06	12·40
−19·5	7·68	20·35	20·93
−20·5	15·04	39·86	40·10

probably due to the impossibility to reproduce the state of the electrode surface in different experiments.

Anyway the visual counting on the micrograph in Fig. 8 leads to a value of $1{\cdot}15 \times 10^9$ nuclei per square centimeter. Even if this datum is not strictly comparable with those listed in Table 3 since it was obtained at a slightly different concentration, it seems to indicate that the equation proposed by Astley *et al.* [5] better describes the present system.

In view of the occurrence of the nucleation phenomena some abnormal characteristics described in the previous section for the linear sweep voltammograms can be tentatively explained according to Hills *et al.* [13] even if mathematical relationships (for example the E_p versus log v or the I_p versus $v^{1/2}$ dependences) are not available because of the complexity of the problem.

Acknowledgements

The authors like to thank Professor P.G. Zambonin for his suggestions and interest in the present work. The electron micrographs were performed in the Centro di Microscopia Elettronica of this University. Work carried out with the financial assistance of the Italian National Research Council (CNR, Roma).

References

[1] T. M. Florence, *J. Electroanalyt. Chem.* **35** (1972) 237.
[2] P. Petak and F. Vydra, *Analyt. Chim. Acta.* **65** (1973) 171.
[3] P. Valenta, L. Mart and H. Rutzel, *J. Electroanalyt. Chem.* **82** (1977) 327.
[4] G. Torsi, *Annali di Chimica* **67** (1977) 557.
[5] D. J. Astley, J. A. Harrison and H. R. Tirsk, *Trans. Faraday Soc.* **64** (1968) 192.
[6] R. Kaischew, A. Scheludko and G. Blinakov, *Ber. Bulg. Akad. Wiss. Physik Ser.* **1** (1950) 137.
[7] A. Scheludko and M. Todorova, *ibid* **3** (1952) 61.
[8] R. Kaischew and B. Mutaftschiew, *Electrochim. Acta* **10** (1965) 643.
[9] D. J. Astley, J. A. Harrison and H. R. Thirsk, *J. Electroanalyt. Chem.* **19** (1968) 325.
[10] G. W. Tindall and S. Bruchenstein, *Analyt. Chem.* **40** (1968) 1051.
[11] W. J. Lorenz, I. Moumtzis and E. Schimdt, *J. Electroanalyt. Chem.* **37** (1971) 121.
[12] G. J. Hills, D. J. Schriffrin and J. Thompson, *J. Electrochem. Soc.* **120** (1973) 157.
[13] *Idem, Electrochim. Acta* **19** (1974) 657.
[14] *Idem, ibid* **19** (1974) 671.
[15] P. Rolland and G. Mamantov, *J. Electrochem. Soc.* **9** (1976) 1299.
[16] M. Gusteri, V. Bartocci, R. Marassi, F. Pucciarelli and P. Cescon, *Annali di Chimica* **66** (1976) 501.
[17] M. Fleischmann and H. R. Thirsk, 'Advances in electrochemistry and electrochemical engineering' (edited by P. Delay and C. W. Tobias) Vol. 3, Interscience, New York (1963).
[18] J. W. Gibbs, 'Collected Works', Longman's Green and Co., London (1928).
[19] O. Volmer, *Z. Phys. Chem.* **119** (1926) 277.
[20] T. Erdey-Gruz and M. Volmer, *Z. Phys. Chem. Abt. A* **157** (1931) 165, 182.
[21] R. M. Garrels and F. T. Gucher, *Chem. Rev.* **44** (1949) 117.
[22] P. Delahay, 'New instrumental methods in electrochemistry' Interscience, New York (1954).
[23] W. L. Miller and A. R. Gordon, *J. Phys. Chem.* **35** (1931) 2785.

[24] G. Mamantov, D. L. Manning and J. M. Dale, *J. Electroanalyt. Chem.* 9 (1965) 253.
[25] T. Berzin and P. Delahay, *J. Amer. Chem. Soc.* 75 (1953) 555.
[26] A. Scheludko and M. Todorova, *Ber. Bulg. Akad. Wiss. Physik Ser.* 3 (1952) 61.
[27] S. Toshev and I. Markov, *Ber. Bunsenges. Phys. Chem.* 73 (1969) 184.
[28] R. Kaishev, S. Toshev and I. Markov, *Bulg. Akad. Sci. Comm. Chem. Dept.* 11 (1969) 463.
[29] R. Kaishev and B. Mutaftschiew, *Bull. Inst. Phys. Chem. (Sofia)* 4 (1954) 105.
[30] *Idem, ibid* 5 (1955) 77.
[31] R. Kaishev, A. Sheludko and G. Bliznakov, *ibid* 1 (1950) 137.
[32] A. Sheludko and G. Bliznakov, *ibid* 2 (1951) 227.
[33] M. Fleischmann, H. R. Thirsk and I. Tordesillas, *Trans. Faraday Soc.* 58 (1962) 1865.
[34] G. A. Gunawardena, G. J. Hills and I. Montenegro, *Electrochim. Acta* 23 (1978) 693.